



# Fatigue strength of single-sided fillet welds in overlapping ultra-high-strength steel sheets

Antti Ahola<sup>1</sup> · Samu Salerto<sup>2</sup> · Timo Loisa<sup>2</sup> · Kalle Lipiäinen<sup>1</sup> · Timo Björk<sup>1</sup>

Received: 1 September 2023 / Accepted: 18 February 2024 / Published online: 4 March 2024  
© The Author(s) 2024

## Abstract

From the manufacturing viewpoint, overlapping thin sheets can provide a substantial geometrical improvement in welded hollow sections compared to butt-welded cross-sectional details. However, the plate eccentricity and non-penetrating fillet welds make the joints susceptible to fatigue failures under transversal cyclic loads. This work experimentally investigates the fatigue strength of overlap joints prepared with gas metal arc welding in the single-sided fillet weld configuration. Fatigue tests were carried out on the lap joints made of S960 ultra-high-strength steel (UHSS) grade under uniaxial constant amplitude axial loading employing both pulsating tension (applied stress ratio of  $R \approx 0$ ) and pulsating compression ( $R \approx -\infty$ ). In addition, the lap joints were prepared with both straight welds (the welds transverse to the loading direction) and inclined welds (the welds with a  $30^\circ$  incliment angle from the transversal direction) to investigate the shear stress effects on the joints' fatigue performance. Plasma butt-welded samples were tested as a reference joint type. For the plasma butt-welded joints, the recommended detail category of FAT71 in the nominal stress system for weld root failures in single-sided butt welds was observed clearly conservative—a mean fatigue strength of  $\Delta\sigma_{c,50\%} = 130$  MPa with a fixed slope parameter of  $m = 3$  was obtained. Compared to the butt-welded joints, a significant decrease in fatigue strength capacity was found in the lap joint specimens with misalignment factors of  $k_m > 3.0$ . The failure locations were also different in joints subjected to the tension and compression loads. The shear load did not majorly contribute to the changes in the fatigue strength capacity compared to the joints subjected to the transversal normal stress.

**Keywords** Fatigue · Welded joint · Overlap joint · Fillet weld · Plate eccentricity

## 1 Introduction

Use of overlapping sheets with single-sided (or double-sided, if accessible) provides a great improvement in reducing requirements for the manufacturing accuracy and tolerances in welded hollow sections compared to butt-welded details. Overlapping joints can be applied in many different structural applications—however, this work was initiated

from the telescopic boom profiles that are usually prepared with butt-welded joints in one or two roll-formed or bent sheets, as demonstrated in Fig. 1b. Such hollow section profiles are usually loaded by global bending moment and shear forces (Fig. 1a) but local contact forces in sliding pads induce locally normal stresses in the transversal direction of welds. In the case of two butt welds at both sides of the hollow section, normally positioned at the lowly stressed area of the major neutral axis of a beam, a high accuracy in the flatness of side planes, profile width, and height should be reached to enable sufficient conditions for the welding preparation. In the case of overlapping sheets, manufacturing tolerances are still important but, e.g., the profile height can be slightly adjusted based on the overlapping length and, on the other hand, the welding jig technologies can be easily adopted to press the overlapping area together to enable geometrical soundness. Particularly in telescopic booms, due to the contact forces of the inner and outer profiles,

---

Recommended for publication by Commission XIII - Fatigue of Welded Components and Structures

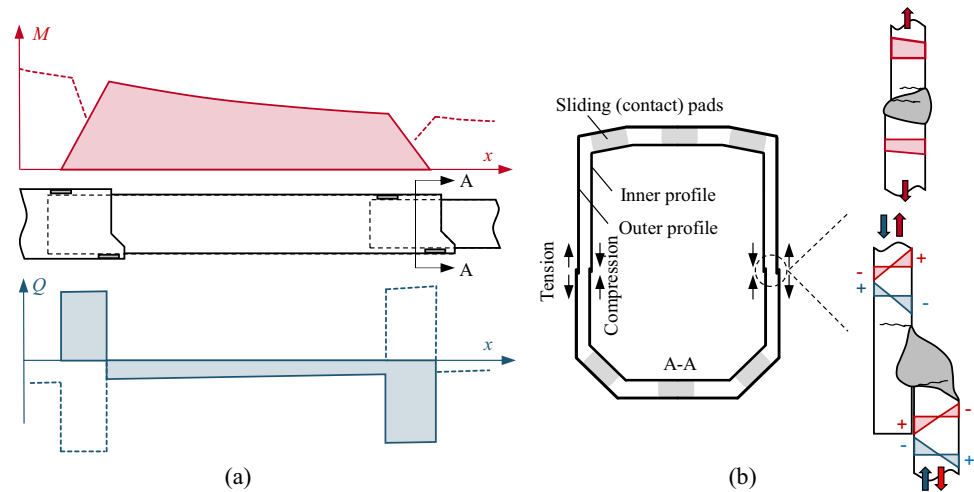
---

✉ Antti Ahola  
antti.ahola@lut.fi

<sup>1</sup> Laboratory of Steel Structures, Lappeenranta-Lahti University of Technology LUT, Yliopistonkatu 34, 53850 Lappeenranta, Finland

<sup>2</sup> Bronto Skylift Oy Ab, Teerivuorenkatu 28, 33300 Tampere, Finland

**Fig. 1** **a** Moment ( $M$ ) and shear force ( $Q$ ) distributions in a telescopic boom, and **b** welded cross-sectional profile with different butt weld and fillet weld configurations



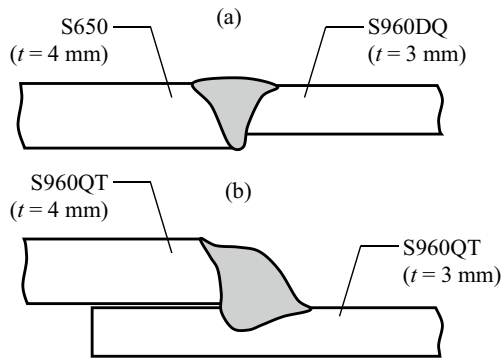
the requirements and tolerances for geometrical shapes and dimensions are important to fulfil functionalities.

In aerial platforms, as in many other high-performing steel structures, the minimization of self-weight in structural elements is one of the key aspects in structural design to increase performance via a reduction in the self-weight to load capacity ratio, as well as an increased reachability. Due to these reasons, the usage of high-strength and ultra-high-strength steels (HSS/UHSS) is a highly attractive solution to reduce weight and has been an industrial standard solution in cranes and lifting equipment. Via the use of HSS and UHSS materials, plate thicknesses can be reduced. This, on the other, creates some challenges from the structural viewpoint. In these investigated hollow sections, the stability of thin sheets against local buckling, global structural stiffness, and fatigue strength of welded connections must be carefully checked [1]. The concerns related to the fatigue of welded connections are involved in reduced stiffness causing higher welding angular deformations and resulting secondary bending stresses under primary membrane stress, in addition to increased cyclic stresses in UHSS constructions.

In thin-walled overlapping sheets, additional concerns are related to the secondary bending stresses induced by the plate eccentricity under axial loading. Under transversal axial tension loading, many studies have shown fatigue failures originating from the weld root to the weld metal in fillet-welded overlapping thin sheets [2–4], mainly due to the root opening moment (Fig. 1b). As a result, low fatigue strength capacities have been obtained, usually corresponding to the detail category of FAT36 in the nominal stress system. Under bending loads, significantly higher fatigue strengths have been found [5, 6], and usually, failures occur at the weld toes. Due to such fatigue failure mode, bending loads also thus benefit from post-weld treatments conducted at weld toes [6] or special weaving

techniques [7]. Regarding the geometrical configuration, the overlap length has not been found as a key factor but the gap size might potentially have an effect on the fatigue strength capacity of these joints [8]. Compared to the transversal axial loads, the fatigue performance of lap joints is also higher for longitudinal normal stresses and shear loads [3, 9]. While some research has been carried out on the fatigue strength capacity of welded overlapping sheets, there is very little scientific knowledge on the effects of different load configurations, i.e., axial tension and compression as well as a combination of normal and shear stresses on the fatigue behavior of these joints. As demonstrated in Fig. 1, both axial tension and compression normal stresses occur in the outer and inner hollow section profiles with the presence of the highest shear loads in the region of the contact area.

The main objective of this work is to develop an understanding on the load and plate eccentricity effects on the fatigue performance of fillet-welded overlapping sheets made of UHSS grades. To meet this objective, an experimental fatigue test campaign was carried out on fillet-welded overlapping joints manufactured from two S960 UHSS grades using gas metal arc welding (GMAW). As a reference joint type for the overlapping sheets, plasma butt-welded joints were manufactured and tested. The fatigue tests were conducted under both axial pulsating tension and compression loads and for joints with both transversal straight welds and inclined welds. The outline of the paper is the following: Section 2 introduces the studied materials, preparation of welded samples, and conducted fatigue tests, Section 3 presents the experimental results in terms of the fatigue test data and failure observations, Section 4 discusses about the main findings of the study and reflects the results on the current knowledge. Finally, Section 5 summarizes the main conclusions drawn from the study.



**Fig. 2** Studied materials in the different specimen types: **a** plasma butt-welded and **b** overlap joints. Section 2.2 presents a detailed description of the joint shape and dimensions

## 2 Materials and methods

### 2.1 Studied materials

The experimental study included a S650 HSS grade and two types of S960 UHSS grades. The studied S650 grade, Strenx 650 MC D, was only used in the plasma butt-welded reference specimens (an HSS grade frequently used in such boom

profiles). To match with actual applications, two different plate thicknesses were chosen for the study; i.e., usually, thinner plates are used in the top flanges experiencing tension under a global bending moment. The plate thicknesses of  $t=3$  mm and  $t=4$  mm were selected for the study. Furthermore, due to the variation in the availability of different types of UHSS grades, two different S960 were included in the study—the plate thickness of  $t=3$  mm was a Strenx 960 MC grade, and the plate thickness of  $t=4$  mm was an Alform 960 X-treme grade (see Fig. 2). In the Plasma butt welding, Normag 2 (ER70S-6,  $\varnothing 1.2$  mm) wire, which is a strength-matching filler wire for mild steels (Table 1), was used. The lap joint specimens (see details in Section 2.2) were prepared with a strength-undermatching filler wire for UHSSs, OK Aristorod 69 (ER110S-G,  $\varnothing 1$  mm), which is a non-copper low-alloyed wire for 700-MPa grade steels. Table 1 and Table 2, respectively, present the mechanical properties and chemical composition of the studied materials.

The experimental work deals with two different types of S960 UHSS grades (Table 1). Of the studied S960 materials, the Strenx 960 MC grade is a low-alloyed UHSS grade manufactured via the direct quenching (DQ) manufacturing route. The Alform 960 x-treme is a quenched and tempered

**Table 1** Mechanical properties of the studied materials.  $t$  is the plate thickness;  $f_y$  and  $f_u$  are the yield/proof strength and ultimate tensile strength of the material, respectively; and  $A$  is the elongation

Material designation	Delivery cond. <sup>a</sup>	ID	$t$ (mm)	Type	$f_y$ (MPa)	$f_u$ (MPa)	$A$ (%)
Strenx 650 MC D [10]	MC	S650	4	Nominal	650	700–850	12
				Mat. cert	706	792	21
Strenx 960 MC [11]	DQ	S960DQ	3	Nominal	960	980–1250	7
				Mat. cert	1016	1088	8
Alform 960 X-treme [12]	QT	S960QT	4	Nominal	960	980–1150	10
				Mat. cert	1004	1026	14
OK Aristorod 69 (ER110S-G) [13]	n/a	ER110	$\varnothing 1$	Typical	730	800	19
DZW Normag 2 (ER70S-6) [14]	n/a	ER70	$\varnothing 1.2$	Typical	450	550	30

<sup>a</sup>MC thermo-mechanically rolled, DQ direct-quenched, QT quenched and tempered, n/a not applicable

**Table 2** Chemical composition of the studied materials (wt-%)

ID	Type	C	Si	Mn	P	S	Al	Cr	Ni	Mo
S650 [10]	Nominal <sup>a</sup>	0.12	0.21	2.00	0.025	0.010	0.015			
	Mat. cert	0.054	0.16	1.64	0.007	0.003	0.035	0.04	0.03	0.005
S960DQ [11]	Nominal <sup>a</sup>	0.12	0.25	1.30	0.020	0.010	0.015			
	Mat. cert	0.080	0.18	1.09	0.009	0.002	0.035	1.12	0.07	0.125
S960QT [12]	Nominal <sup>a</sup>	0.12	0.50	1.70	0.015	0.020	0.020	1.50	2.00	0.70
	Mat. cert	0.087	0.115	1.68	0.006	0.005	0.059	0.970	0.460	0.231
ER110 [13]	Typical	0.089	1.54	0.53	0.01	0.01		0.26	1.23	0.24
ER70 [14]	Typical	0.06–0.15	0.80–1.15	1.40–1.85	0.025	0.035		0.15	0.15	0.15

<sup>a</sup>Maximum values, except for aluminum (minimum content)

UHSS grade. The mechanical properties of these two steels are rather similar but behave differently under deposited heat input due to the welding. In general, direct-quenched UHSS grades usually suffer from the strength reduction (material softening) at the heat-affected zone (HAZ) due to the loss of bainitic-martensitic microstructure produced via the quenching process. Meanwhile, QT steels, due to their higher share of alloying elements, usually experience an increase in hardness at the HAZ, particularly in weldments with higher cooling rates, i.e., low heat inputs [15]. Due to these reasons, the minimum allowable cooling rate (and maximum allowable heat input) is more critical in DQ steels than in QT steels, while requirements for maximum allowable cooling rate must be particularly satisfied in QT steels. The hardness profiles of the butt-welded and lap-welded specimens have been shown in Section 2.2.

## 2.2 Preparation of the test specimens

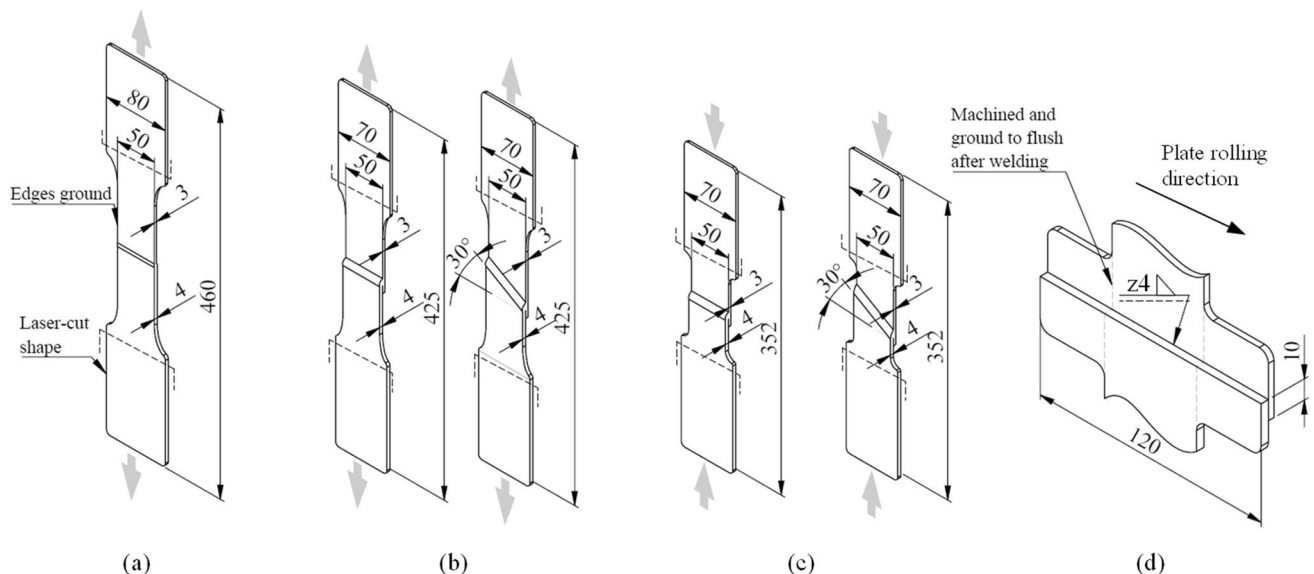
Two different joint types were investigated: plasma butt-welded specimens (the reference case) and overlap joints prepared with single-sided fillet welding. The plasma butt-welded specimens were prepared by welding two 800-mm × 400-mm sheets with thicknesses of 3 mm (S960DQ) and 4 mm (S650) in the flat (PA) position (Table 4) using a mechanized welding unit. Before welding, the plates were clean-blasted. From the butt-welded sheets, the specimens were extracted by laser cutting coupon shape specimens (Fig. 3a). The fillet-welded lap joint specimens were manufactured as individual sheets with welding run-on and run-off parts outside the investigated joint area (Fig. 3d). The

lap joint specimens had both 90° angle (weld transverse to the loading direction, hereafter referred as specimens with “straight welds”) and 60° angle to the uniaxial loading direction (hereafter referred as specimens with “inclined welds”), as shown in Fig. 3b and c. The test matrix has been presented in Table 3. For the lap joints tested under compression, a smaller specimen length, compared to the tensile-tested specimens, was applied to avoid unfavorable flexural buckling of the specimens under compressive loading.

The fillet welding was conducted using the GMAW process. To demonstrate similar welding conditions usually applied in actual beam profiles (Fig. 1), a horizontal-vertical (PB) welding position, with the specimens aligned in the vertical position, was chosen for the small-scale specimens as shown in Fig. 4. The specimens with inclined welds were also prepared at the same welding position; i.e., the specimen was rotated (in-plane) to receive horizontal welding direction. The joints were clamped to the welding jig with four spring clamps—two located at the joint area and two located at both ends of the specimens. The main welding parameters (as per the welding procedure specification, WPS) have been presented in Table 4.

## 2.3 Hardness measurements

Hardness measurements were conducted on both plasma butt-welded joint and fillet-welded lap joint using a 1-kg Vickers testing (HV1), together with scanning electron microscopy (SEM) on the local geometry at the fatigue-critical locations of the joints. The measured hardness distributions are presented in Figs. 5 and 6 for the plasma



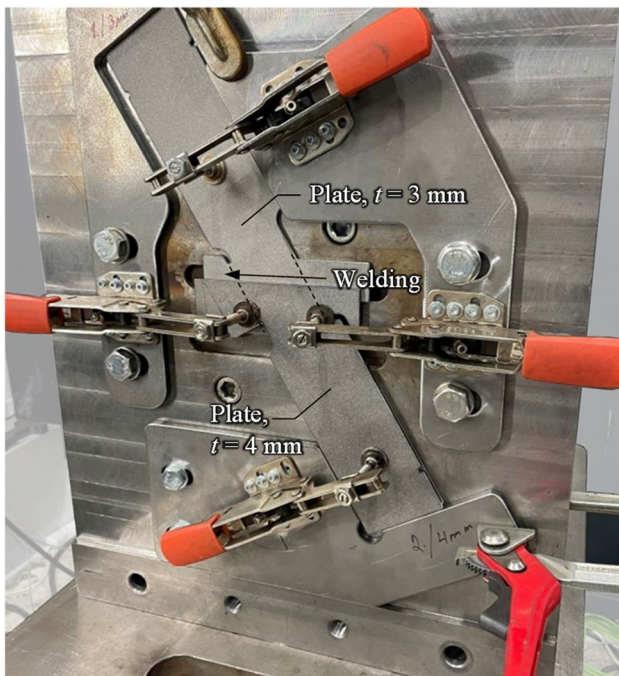
**Fig. 3** Shape and dimensions (in millimeters) of the studied joint types: **a** plasma butt-welded specimens, lap joint specimens with the straight and inclined welds tested **b** in tension and **c** in compression, and **d** laser cut shape for the lap joint specimens in welding

**Table 3** Test matrix of the fatigue test campaign. *R* is the applied stress ratio of external loading and *n* is the number of specimens

Joint type	Specimen (Fig.)	Welding process	Load type <sup>a</sup>	<i>n</i>	Specimen IDs <sup>b</sup>
Butt joint	3a	Plasma	Tension ( <i>R</i> ~0)	8	S96_S65_PBWJ_1–8
Lap joint—straight weld	3b	GMAW	Tension ( <i>R</i> ~0)	7	S96_SLJ_1–7
Lap joint—straight weld	3c	GMAW	Compression ( <i>R</i> ~-∞)	7	S96_SLJ_11–17
Lap joint—inclined weld	3b	GMAW	Tension ( <i>R</i> ~0)	6	S96_SLJ_21–26
Lap joint—inclined weld	3c	GMAW	Compression ( <i>R</i> ~-∞)	5	S96_SLJ_32–36

<sup>a</sup>See further details from Section 2.4

<sup>b</sup>Fatigue test results and details of each specimen have been presented in Appendix 1



**Fig. 4** Lap joint specimen with the inclined weld in the welding jig

butt-welded and fillet-welded specimens, respectively. In the plasma butt-welded joints, the S650 base metal reached a hardness of 280 HV, while the base metal hardness of the


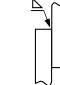
S960QC was around 350 HV. In the plasma butt-welded specimens, the strength-undermatching filler wire for HSSs and UHSSs was used (equivalent to S355 steel grades). Due to these reasons, a lower hardness can be observed for the weld metal than both base metals. Both materials suffered from hardness reduction at the fine-grained HAZ, with the values being rather similar in both S650 and S960DQ sides, but obviously, the hardness drop and corresponding strength reduction are more severe in the studied UHSS grade compared to the base metal strength.

### 2.4 Fatigue testing and instrumentation

The fatigue tests were carried out using a servohydraulic 150-kN force-controlled fatigue testing machine under uniaxial loading with constant amplitude sinusoidal waveforms (Fig. 7). The test frequency was adjusted as per the expected number of cycles to failure and it was between  $f = 1.0$  and 2.0 Hz. Both uniaxial tension and compression loads were applied in the tests with the aim of having minimum load (in the tension tests) and maximum load (in the compression tests) equal to zero, corresponding to the load conditions in the outer and inner profile, respectively. However, due to the practical reasons, a cylinder preload of  $F_{min} = 1$  kN (tension tests) and  $F_{max} = -1$  kN (compression tests) was applied to avoid peak values equal to zero. The resulting *R* values have been reported in Appendix 1 for each tested specimen.

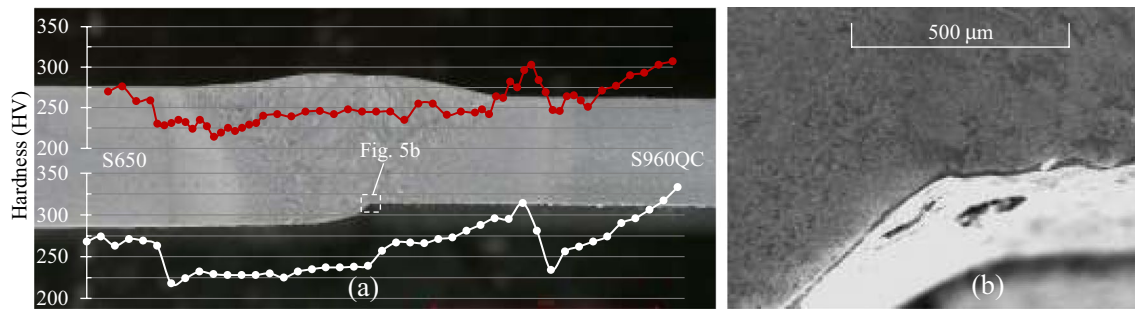
**Table 4** Welding parameters of the test specimens. *U* is the welding voltage, *I* is the welding current,  $v_{wire}$  is the wire feed rate,  $v_{travel}$  is the torch travel speed, CTWD is the contact tip to work distance, *Q* is the

welding heat input, and  $t_{8/5}$  is the cooling time from 800 to 500° as per the EN 1011–1 and EN 1011–2 standards [16, 17]

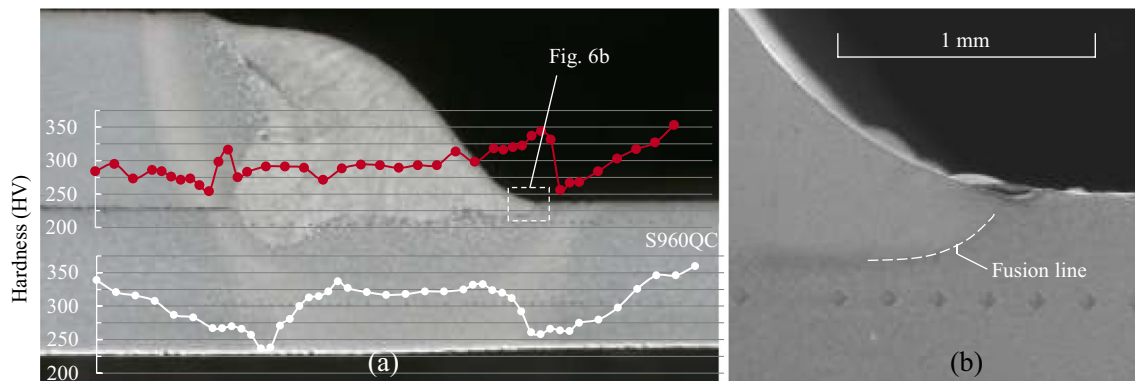
Joint type	Welding position	Process	<i>U</i> (V)	<i>I</i> (A)	$v_{wire}$ (m/min)	$v_{travel}$ (mm/s)	CTWD (mm)	<i>Q</i> (kJ/mm)	$t_{8/5}$ <sup>a</sup> (s)
Butt weld	PA 	Plasma	25.5–30	160–190	0.5–1.5	6.2–7.2	10–15	0.39–0.48	18–26
Lap joint	PB 	GMAW	24.5	230–240	10.5	15.5	16	0.3	10

<sup>a</sup>For the *t* = 3-mm plate with the thermal efficiency factors of *k* = 0.6 (plasma) and *k* = 0.8 (GMAW) and shape factors of  $F_2 = 0.9$  (for both joint types)



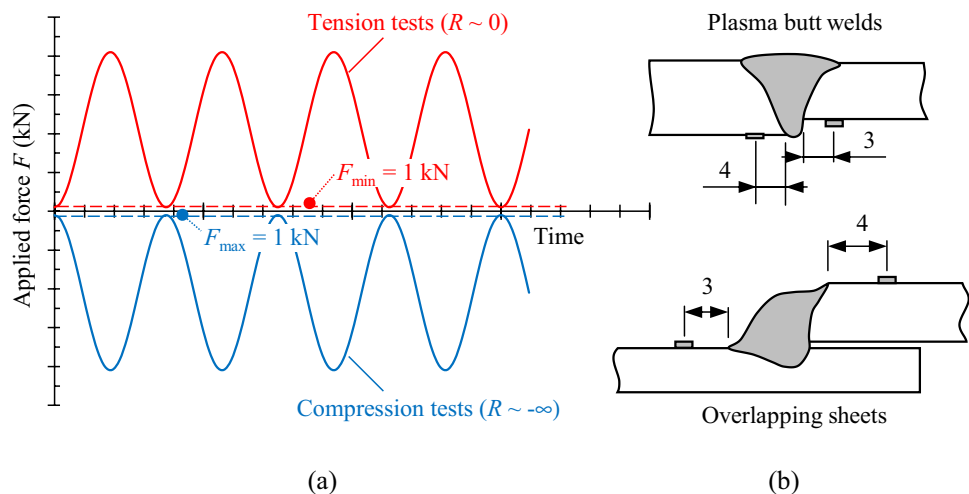


**Fig. 5** **a** Hardness distribution for the plasma butt-welded joint and **b** SEM image on the fatigue-critical location of the weld root



**Fig. 6** **a** Hardness distribution for a fillet-welded lap joint, and **b** SEM image on the weld fusion line at the weld toe position

**Fig. 7** **a** Applied load types in the fatigue tests and **b** positioning of the strain gages.



The fatigue tests were carried out using three different load levels. These load levels were adjusted to have a targeted number of cycles to failure between  $N_f = 5000$  and 100,000, corresponding to the reasonably low number of fatigue load cycles in typical lifting boom structures. However, in all tests, these values could not be reached due to the material and geometrical limitations. In the plasma butt-welded specimens, the allowable load level was limited

by the material strength of the S650 grade, and the maximum load peak value was limited to up to 90% of the yield strength of the material. On the other hand, in the compressed lap joints, the flexural buckling capacity of the specimens limited the allowable compressive load to  $F_{\min} = -45$  kN. Due to these limitations, the lowest number of targeted cycles was not completely reached in these specimens. During the fatigue testing, the minimum and maximum values

of the applied force (force transducer), strains, and displacements were monitored at 1-min intervals. The fatigue tests were stopped if a certain displacement limit (due to the crack growth and increased flexibility/instability) was reached. In the tensile-tested specimens, this signified a total rupture of the specimens, but the compression tests stopped before total rupture. However, substantial fatigue cracks were observed in these specimens (see also Fig. 8 in Section 3.1).

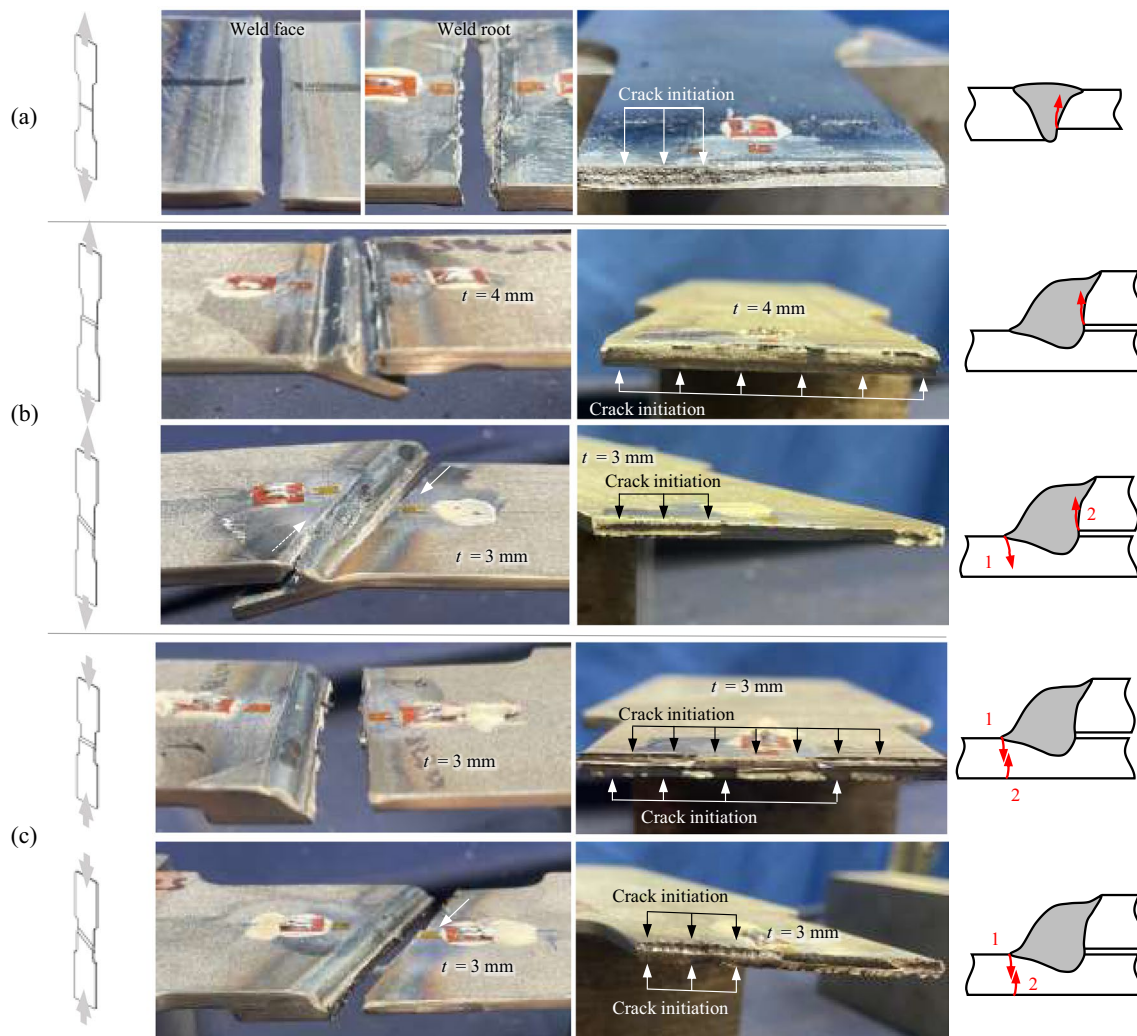
Each specimen was equipped with two strain gages—one located in the  $t=3$ -mm plate, and one located in the  $t=4$ -mm plate, as shown in Fig. 7b. In the plasma butt-welded specimens, the strain gages were positioned at the root side of the plates which was the expected failure location. In the lap joint specimens, due to the inaccessibility to the weld root, the strain gages were positioned close to the weld in the  $t=4$ -mm plate, as well as next to the weld at the top of the  $t=3$ -mm plate. Following the IIW Recommendations, strain

gages with a measuring grid length of 0.6 mm were used (given limitation  $<0.2t$ ) [18]. By means of the strain gages, the structural strains (and eventually structural stresses) were measured by applying Young's modulus of  $E=210$  GPa. These values were used in the evaluation of the fatigue test data (see detailed description on the stress evaluation in Section 3.2).

## 3 Results

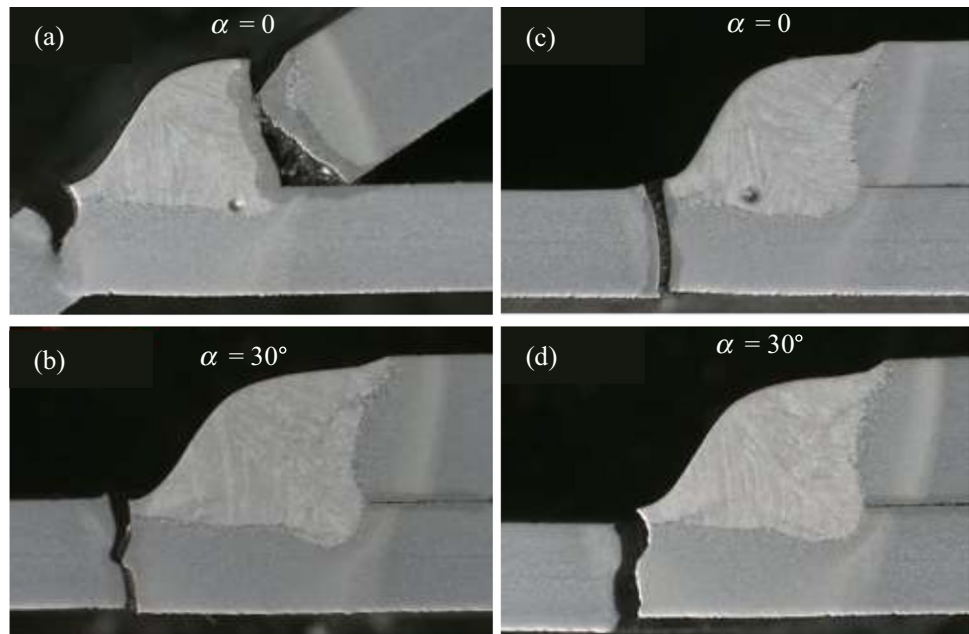
### 3.1 Observations on fatigue failure locations

The failure locations in each joint type are presented in Fig. 8 with the photographs of the failed specimens and fracture surfaces. The cross-sectional fracture paths in the lap joints are presented in Fig. 9. As expected, in the



**Fig. 8** Fracture images on failed specimens: **a** a plasma butt-welded joint, **b** lap joints tested under tensile load, and **c** lap joints tested under compressive load

**Fig. 9** Cross-sectional images on the fracture paths in the lap joint specimens: **a, b** specimens tested in tension and **c, d** specimens tested in compression



plasma butt-welded joints, the failures occurred in the weld root at the S960 side in the  $t=3$ -mm plate (Fig. 8a). In the lap joint specimens, the fatigue failure location depended on the load conditions. The tensile-loaded specimens with the straight welds failed from the weld root (Figs. 8b and 9a) and cracks grew through the weld and/or  $t=4$ -mm plate. In these specimens, high secondary bending stresses occurred with opening bending stress at the root side of the  $t=4$ -mm plate (see also Section 3.2 for the stress analysis and fatigue test results). In those with the inclined welds and tested under tensile loading, combinations of the toe ( $t=3$  mm) and root ( $t=4$  mm) cracking were found (Fig. 8b). Based on the observed crack sizes in the failed specimens, the failures first originated at the weld toe of the  $t=3$ -mm plate and subsequently cracks grew at the weld root.

The lap joints, fatigue tested in compression, failed from the weld toe position. As confirmed by the strain gage measurements, bending moment, causing compressive stresses at the weld toe of the  $t=3$ -mm plate and at the weld root, was present in these specimens. However, the fatigue crack also grew to approximately half of the plate thickness (see Fig. 9c) after which fatigue cracks initiated from the base metal of the bottom of the plate. In some tests, the failure criterion was reached and tests were stopped before observing the cracks originating from the bottom of the plate. Similar behavior was observed in the specimens subjected to combined axial and shear load (Fig. 9c and d). Using the SEM, it was identified that the failures at the bottom of the  $t=3$ -mm

plate (Fig. 9c, d) originated from individual surface defects associated with the blast cleaning process prior to the welding preparation.

### 3.2 Fatigue test results

The fatigue test results (Sections 3.2.1–3.2.3) were evaluated as per the nominal and structural stress system. For the overlap joints, similar to other joint types prepared with fillet welding, the FAT classes for the nominal stresses cover misalignment factors up to  $k_m=1.25$ . Additional macrogeometric stresses should be considered by applying effective misalignment factors (see Eq. (2)) [18]. For lap joints, however, this is only recommended for plate stresses excluding its consideration for the weld root failures and corresponding stresses at the weld root in lap joints [18]. Since the objective of the study is to compare different joint configurations (butt welds and fillet-welded overlap joints), macrogeometric stresses were excluded in the evaluation. Nevertheless, for the overlap joints with the straight welds, the structural stresses were also obtained to consider the macrogeometric stresses caused by the joint eccentricity and welding-induced angular distortions. In this way, macrogeometric stresses and joint eccentricities were evaluated with respect to the FAT classes in the nominal stress system [18]

The nominal (membrane) stresses were obtained based on the applied axial load and cross-sectional area in both specimens with the straight and inclined welds. In this context, the cross-sectional area refers to the plate in which failures



occurred. In the tensile-tested lap joint specimens with the straight welds and failing from weld root, the nominal stresses were calculated at the  $t=4$ -mm plates. In all other specimens, fatigue failures were observed at the  $t=3$ -mm plate and, consequently, the stresses were obtained in this plate. In butt-welded details, the  $S-N$  curves for nominal stresses cover a misalignment factor of  $k_m=1.3$  (due to angular misalignment/distortion and plate offset) [18]. The misalignment factor can be obtained as follows:

$$k_m = \frac{\Delta\sigma_s}{\Delta\sigma_{nom}}, \tag{1}$$

where  $\Delta\sigma_s$  is the structural stress range comprised of the membrane (due to the axial forces) and bending stresses (due to the misalignments) and  $\Delta\sigma_{nom}$  is the nominal stress. If the misalignment value is exceeded, misalignments should be considered in the determination of nominal stresses with an effective misalignment factor as follows:

$$k_{m,eff} = \frac{k_m}{k_{m, \text{already covered}}} = 1.3, \tag{2}$$

and (effective) nominal stress range (macrogeometric stress) is determined as follows:

$$\Delta\sigma_{nom,eff} = k_{m,eff} \Delta\sigma_{nom}. \tag{3}$$

The structural stresses were obtained for the specimens with the perpendicular welds, i.e., the plasma butt-welded joints and overlap joints with the straight welds. The obtained structural stresses were obtained at the location of the failure (see Section 3.1):

- Plasma butt-welded specimens: structural stress at the weld root at the  $t=3$ -mm plate
- Lap joint specimens under tension: structural stress at the weld root at the  $t=4$ -mm plate
- Lap joint specimens under compression: structural stress at the weld toe at the  $t=3$ -mm plate

The structural stresses were obtained based on the strain gage measurements, determined as follows:

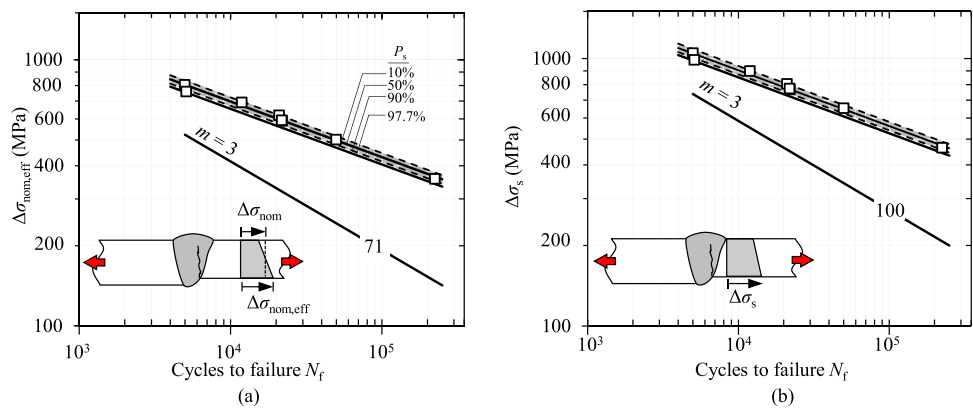
$$\Delta\sigma_s = \Delta\sigma_m + \Delta\sigma_b, \tag{4}$$

where  $\Delta\sigma_m$  and  $\Delta\sigma_b$  are the membrane and bending stress ranges, respectively. For the different joint types and fatigue test series, the  $S-N$  curves were obtained using the standard procedure for the regression analyses, i.e., the number of cycles  $N_f$  as a dependent (unknown) variable and applied stress range  $\Delta\sigma$  as an independent variable (known variable). Both natural slope parameters ( $m_{free}$ ) and fixed slope parameters ( $m=3$ ) were applied in the evaluation.

### 3.2.1 Plasma butt-welded joints

Fatigue test results of the plasma butt-welded specimens are presented in Fig. 10 and Table 5 in terms of the nominal and structural hot-spot stress systems using the natural slope parameter fitted to the test data. For the nominal stresses, a detail category of FAT71 was selected as the standardized reference curve [18]. FAT71 is intended for the butt weld details welded from one side and failing from the weld root but inspected by appropriate NDT testing including visual inspection (no defects/initial cracks at the weld root). For the structural hot-spot stress

**Fig. 10** Fatigue test results of the plasma butt-welded joints (reference series) in **a** the nominal stress and **b** structural stress systems



**Table 5**  $S-N$  curve parameters for the plasma butt-welded joints using fixed ( $m=3$ ) and natural slope parameters

Stress criterion	Fig	Fixed, $m=3$ (Appendix 2)		Natural slope, $m_{free}$		
		$\Delta\sigma_{c,50\%}$ (MPa)	$\Delta\sigma_{c,97.7\%}$ (MPa)	$\Delta\sigma_{c,50\%}$ (MPa)	$\Delta\sigma_{c,97.7\%}$ (MPa)	$m_{free}$ (-)
Nominal	10a	130	91	230	216	4.78
Structural	10b	170	119	299	281	4.78

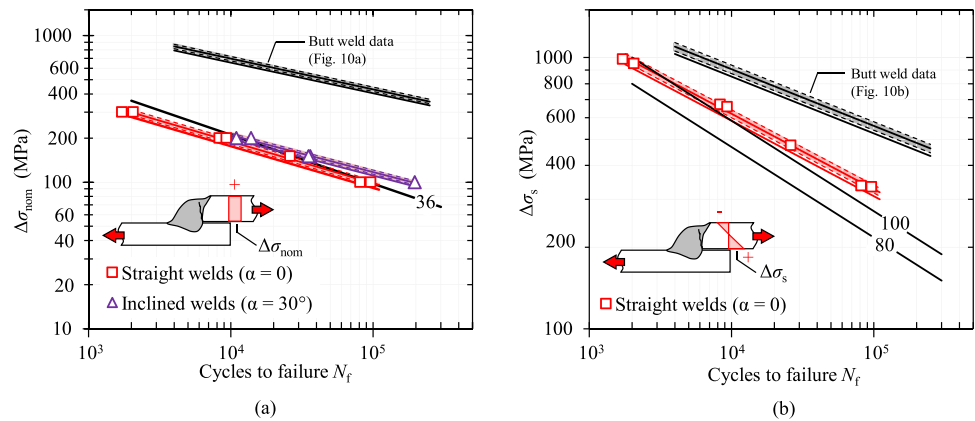
method, the design curve is FAT100 (for as-welded condition proved to be free from significant flaws by NDT). It is worth noting that FAT100 is only applicable for the toe failures in butt-welded joints (usually in a case of welding from both sides), but here, it is selected to be presented as a reference curve for the studied plasma butt-welded joints, since the secondary bending stresses at the root side were measured. In addition, currently, there is not a recommended design curve for the root failures in butt joints in the structural stress system. The notation applied in Fig. 10a for the different survival probabilities of  $P_s = 10\%$ , 50%, 90%, and 97.7% is applied hereafter in the  $S-N$  data plots for the lap joints (Figs. 11 and 12 in Sections 3.2.2 and 3.2.3, as well as Figs. 13 and 14 in Appendix 2). As can be seen from Fig. 10 and Table 5, the obtained fatigue strengths clearly exceed the recommended design values (FAT71 and FAT100).

Appendix 2 provides the  $S-N$  curve plots applying the fixed slope parameters.

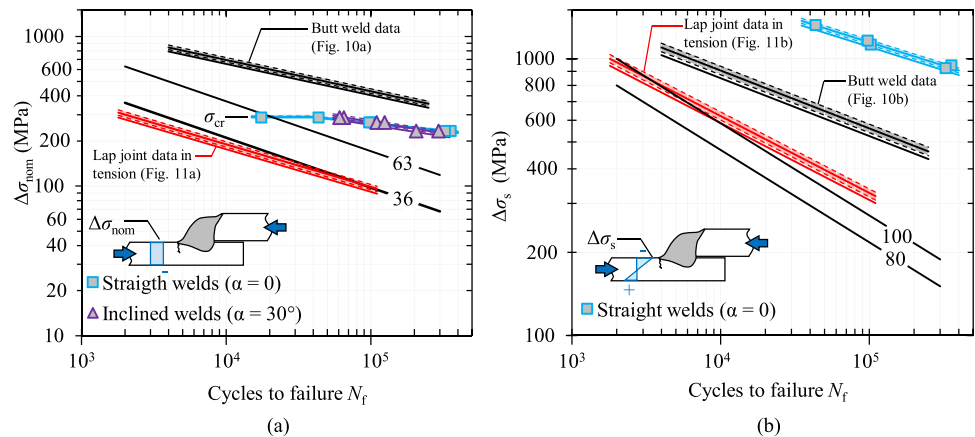
### 3.2.2 Lap joints under tension load

The fatigue test results of the lap joint specimens under tension are presented in Fig. 11 (with natural slope parameters) and Table 6. The fatigue test data of the plasma butt weld joints are presented as a comparison. Due to the unclear definition of structural stresses for the joints subjected to combined normal and shear stresses, the inclined welds are only presented in terms of the nominal stresses in Fig. 11a, referring to the principal (normal) stress at the plate. The fatigue strength capacity of the lap joints is much lower than that of the reference butt weld specimens—and the fatigue strength of the lap joints does

**Fig. 11** Fatigue test results of the overlap joints with the straight ( $\alpha = 0^\circ$ ) and inclined ( $\alpha = 30^\circ$ ) welds under tensile load in **a** the nominal stress system and **b** the joints with the straight welds in the structural stress system



**Fig. 12** Fatigue test results of the overlap joints with the straight ( $\alpha = 0^\circ$ ) and inclined ( $\alpha = 30^\circ$ ) welds under compressive load in **a** the nominal stress system and **b** the joints with the straight welds in the structural stress system



**Table 6**  $S-N$  curve parameters for the lap joints under tensile loading using fixed ( $m = 3$ ) and natural slope parameters

Stress criterion	Joint type, $\alpha$ ( $^\circ$ )	Fig	Fixed, $m = 3$ (Appendix 2)		Natural slope, $m_{free}$		
			$\Delta\sigma_{c,50\%}$ (MPa)	$\Delta\sigma_{c,97.7\%}$ (MPa)	$\Delta\sigma_{c,50\%}$ (MPa)	$\Delta\sigma_{c,97.7\%}$ (MPa)	$m_{free}$ (-)
Nominal	0	11a	33	27	42	39	3.51
	30	11a	39	31	55	52	3.98
Structural	0	11b	108	87	142	134	3.60

not reach the lowest detail category (FAT36) for welded steel components when the macrogeometric stresses are not considered. The misalignment factors, due to the plate eccentricity and angular distortion (accounts for both factors in lap joints), were  $k_m = 3.16\text{--}3.35$  (see Appendix 1). By evaluating the test results by using the structural stresses, the fatigue test data is closer to the reference (butt-welded) specimens. For the structural weld stress system, FAT80 has been proposed by Fricke [19], although this recommendation has not reached official standards and design codes. However, the fatigue test data is above the FAT80 curve with a reasonable margin for conservative fatigue assessments. FAT100 seems to be conservative at the intermediate life regime but shows unconservative results at the low-cycle regime.

### 3.2.3 Lap joints under compression load

The fatigue test results of the lap joints under compressive load are presented in Fig. 12 (with natural slope parameter) and Table 7. The fatigue test data of these specimens were evaluated based on the nominal stresses at the  $t = 3\text{-mm}$  plate. This also applies to the inclined welds for which nominal stress refers to the principal (normal) stress in the plate. For the lap joint with the straight welds, misalignment factors of  $k_m = 3.96\text{--}4.65$  were measured, resulting in a high fatigue strength in the structural stress system (Fig. 12b). The fatigue testing and  $S\text{--}N$  curves are limited by the critical stress,  $\sigma_{cr}$ , limiting the compressive loading by the flexural buckling of the test specimen. This can be seen by the knee-point at the stress level of  $\Delta\sigma_{nom} = 280\text{--}300$  MPa (at around 50,000 cycles, Fig. 12a). In terms of the nominal stresses, both specimens with the straight ( $\alpha = 0$ ) and inclined ( $\alpha = 30^\circ$ ) welds had similar fatigue strength capacity in the intermediate life (at  $1\text{--}4 \times 10^5$  cycles) and fit into the same scatter band. Nevertheless, Table 7 and Fig. 12 show fatigue strengths obtained individually for both data sets. Applying the nominal stress criterion, it can be observed that under compressive loading, the lap joints under compressive loading had higher fatigue strength capacity than the lap joints under tensile loading but still lower than in the plasma butt-welded reference specimens. However, considering the misalignments by structural stresses, the fatigue strength of the lap joints under compression was much higher than that of reference specimens and lap joints under tension.

## 4 Discussion

In this study, the fatigue strength capacity of overlapping UHSS sheets welded with single-sided fillet welds was experimentally determined with the aim of studying the load condition effects on the fatigue and failure behavior of these joints. The plasma butt-welded joints were regarded as a reference joint type, for which high fatigue strength capacity, up to a mean fatigue strength of 130 MPa (Table 5), was obtained in the nominal stress system. Such high fatigue strength capacity could be expected since the applied plasma welding procedure provided flawless root geometry (Fig. 5) with a reasonably good transition from the  $t = 3\text{-mm}$  plate to the weld metal.

Compared to the plasma butt-welded joints, the fatigue strength capacities of lap joints under both axial tension and compression were obviously much lower. This was particularly the case for the tension-loaded joints for which the plate eccentricity of overlapping sheets caused secondary bending stresses (opening weld root) and failures originated from the weld root through the welds. When using nominal stresses, the mean fatigue strength ( $m = 3$ ) of the lap joints was 33 MPa, and thus, even the lowest detail category of FAT36 does not necessarily provide conservative assessments when the misalignments are not considered. The observed failure locations (Figs. 8, 9) and obtained fatigue capacities (Fig. 11) were in line with those found in the prior investigations [2–9]. However, due to the high magnitude of secondary bending stresses with misalignment factors equal to  $k_m = 3.16\text{--}3.35$ , which are also highly dependent on the plate thicknesses, fatigue assessments using the nominal stress system are not necessarily well-suited for such joint types without experimental verifications.

To evaluate the fatigue strength capacity of lap joints failing from the weld root under tensile loading, the structural weld stresses were obtained, and fatigue test data was evaluated using this data (Fig. 11b). The results with the structural weld stresses showed consistency with the FAT80 design curve earlier suggested for structural weld stress system in fillet weld joints failing from weld root [19]. This finding has important implications for developing fatigue assessment methodology for considering different magnitudes of secondary bending stresses in such overlapping joints. If the results evaluated by the structural stresses are converted to the nominal stress system via the

**Table 7**  $S\text{--}N$  curve parameters for the lap joints under tensile loading using fixed ( $m = 3$ ) and natural slope parameters

Stress criterion	Joint type, $\alpha$ ( $^\circ$ )	Fig	Fixed, $m = 3$ (Appendix 2)		Natural slope, $m_{free}$		
			$\Delta\sigma_{c,50\%}$ (MPa)	$\Delta\sigma_{c,97.7\%}$ (MPa)	$\Delta\sigma_{c,50\%}$ (MPa)	$\Delta\sigma_{c,97.7\%}$ (MPa)	$m_{free}$ (-)
Nominal	0	12a	105	64	195	192	9.74
	30	12a	103	78	170	162	6.50
Structural	0	12b	446	313	691	664	5.90

effective misalignment factor ( $k_{m, \text{already covered}} = 1.25$  for fillet weld joints), the results suggest characteristic fatigue strength of  $\Delta\sigma_{c, 97.7\%, \text{corr.}} = 87 \text{ MPa}/1.25 = 70 \text{ MPa}$  (Table 6). Thus, fatigue class FAT63 could be applicable to the root failures in overlapping sheets with single-sided fillet welds. For joints with double-sided fillet welds in overlapping sheets, FAT36 has been proposed in the IIW Recommendations [18]. However, a consideration of the misalignment effects is not addressed. Further validations should be conducted on different magnitudes of eccentricity, e.g., by increasing and/or decreasing the eccentricity by forming the sheets or varying the plate thicknesses. Furthermore, the thickness and resulting stress gradient effects should also be further evaluated.

By reviewing experimental data from the literature, the vast majority of fatigue testing has been carried out using either axial tension or bending loading. This work also contributed to understanding the effects of compressive loads on the fatigue behavior of lap joints. Under axial compression, plate bending resulting from the plate eccentricity causes compression stresses at both weld root and weld toe with the superposition from the compressive axial stress. In the studied joints, the primary failures occurred at the weld toe position (at the  $t = 3\text{-mm}$  plates, Figs. 8, 9). Compared to the axial tension tests, clearly higher fatigue strength capacity was obtained for the lap joints tested under compression, with the mean fatigue strength of 105 MPa and 103 MPa ( $m = 3$ ) for the specimens with the straight and inclined welds, respectively. In addition, the results indicated shallower slopes when the natural slope parameters were fit to the data (Table 7). It was also found that the flexural buckling capacity of thin-walled specimens limited the load-carrying capacity, which could be identified by the knee-point at the low-cycle fatigue regime at the stress range level of 280–300 MPa (Fig. 12). It is also worth mentioning that the specimens were welded in the vertical position (Fig. 4 and Table 4), corresponding a normal welding procedure in hollow sections. With such welding position, smooth transition was obtained for the fatigue-critical weld toe favoring high fatigue performance in the case of toe failure under compression loads. The results of this study did show neither any significant decrease nor increase in the fatigue strength capacity of the overlap joints under combined axial and shear loading (Figs. 11, 12). This finding is in line with those observations found in pure axial and shear load conditions [3]. Consequently, these results suggest that the location experiencing the highest normal axial stresses is the most fatigue-critical region in hollow section profiles with overlapping sheets subjected to transversal loads in addition to global bending moment.

Compared to the plasma butt-welded joints, the lap joint specimens obviously show lower fatigue strength capacity. However, this observation is limited to the plasma butt-welded joints studied in this work. For the studied samples, sufficient weld penetration was obtained providing a reasonably good transition over the plate eccentricity at the weld root (Fig. 5a). For gas

metal arc-welded longitudinal seams, weld quality particularly at the weld root is potentially different affecting the fatigue strength in the studied butt weld configuration. In boom structures, however, primary cyclic stresses are induced by the global bending moment, and usually, these welds are positioned close to the neutral axis of the profile. If transversal normal stresses can be kept at a reasonable limit, lap joints are viable options for such boom structures. Based on the results of this study, particular attention should be paid to the axial tension load conditions, causing an opening bending moment at the weld root of the lap joint. Depending on the applied web shape and plate thicknesses in such hollow sections, the magnitude of secondary bending stresses might highly vary. Due to this reason, fatigue assessment should be preferably conducted using structural weld stresses, considering the secondary bending stresses.

## 5 Conclusions

The present investigation experimentally studied the fatigue strength of welded thin-walled connections in the plasma butt-welded and fillet-welded lap joint configurations in the context of hollow sections experiencing various load conditions in telescopic boom profiles. Based on the experimental findings, the following conclusions can be drawn.

- The plasma butt-welded reference specimens showed the highest fatigue strength capacity amongst the tested series of butt welds and lap joints. The applied plasma welding procedure successfully resulted in fully penetrating welds in the I groove with two different plate thicknesses ( $t = 3 \text{ mm}$  and  $t = 4 \text{ mm}$ ). The weld root geometry was reasonably smooth without any root defects and fatigue test results were clearly above the recommended fatigue classes—FAT71 and FAT100 for the nominal and structural stress systems, respectively.
- The lap joint specimens under tension loading showed low fatigue strength capacity due to the plate eccentricity with the characteristic fatigue strength in the nominal stress system being  $\Delta\sigma_{c, 97.7\%} = 27 \text{ MPa}$  ( $m = 3$ , without considering the macrogeometric stresses due to the plate eccentricity). To account for the high axial misalignment, this joint type favors the use of the structural stress system—by considering the joint eccentricity in the evaluation of structural stresses ( $k_m = 3.16\text{--}3.35$ ), the study showed that FAT80 could be conservatively applied for assessing the fatigue strength of overlapping joints under tension loading. For the lap joint specimens under tension, the effective misalignment factors thus were  $k_{m, \text{eff}} = 2.5\text{--}2.7$  for the specimens with the straight welds and, based on the results, FAT63 could be suggested if the plate misalignments are considered in the macrogeometric stresses.
- Compressive loading causes bending moment at lap joints inducing compressive normal stresses at the weld toe and



weld root, causing failures originating from the weld toe under compressive stress at the plate surface. Without considering the misalignments, the characteristic fatigue strength was  $\Delta\sigma_{c,97.7\%} = 64$  MPa ( $m=3$ ) for the specimens with the straight transversal welds in the nominal stress system. Meanwhile, the misalignment factors were higher for these compressive load conditions, i.e.,  $k_m = 3.96\text{--}4.62$ , due to the lower plate thickness at the failure location ( $t=3$  mm).

- The fatigue test results of the specimens with the inclined welds suggested that the consideration of shear load in a combination of normal stresses is not necessarily important in the lap joint specimen since equal or higher fatigue strength capacity was obtained for the specimens with the inclined welds compared to the specimens with the welds perpendicular to the loading direction.

## Appendix 1. Fatigue test data

**Table 8** Fatigue test data points

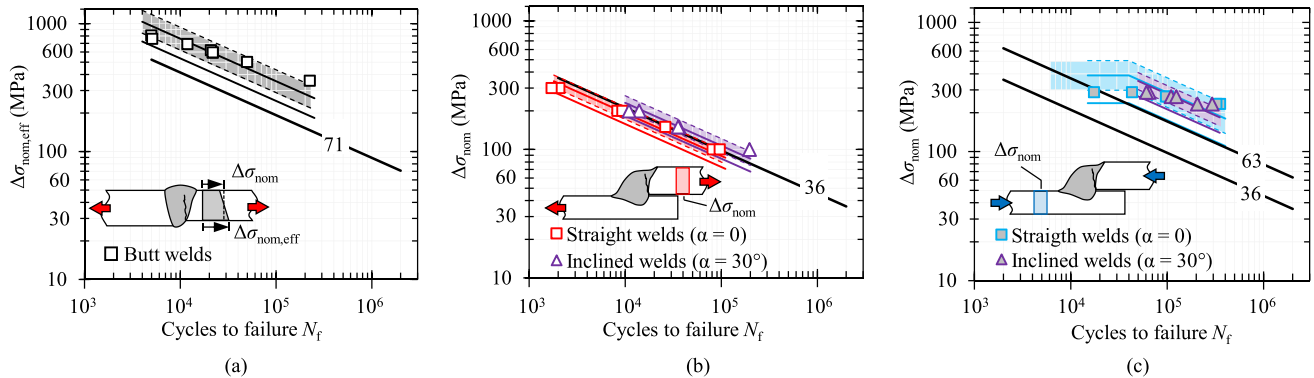
Specimen ID	Joint type	Load type	$R$	$F_{\max}$ (kN)	$F_{\min}$ (kN)	$\Delta F$ (kN)	$\Delta\sigma_{m,1}, t=4$ mm (MPa)	$\Delta\sigma_{m,2}, t=3$ mm (MPa)	$k_m^a$ (-)	$N_f$ (cycles)
S96_65_PBWJ_1	Plasma butt weld	Tens	0.01	68.5	1	67.5	337.5	450	1.70	21,840
S96_65_PBWJ_2	Plasma butt weld	Tens	0.01	83.5	1	82.5	412.5	550	1.46	21,342
S96_65_PBWJ_3	Plasma butt weld	Tens	0.02	56.5	1	55.5	277.5	370	1.25	225,188
S96_65_PBWJ_4	Plasma butt weld	Tens	0.01	101	1	100	500	667	1.35	11,911
S96_65_PBWJ_5	Plasma butt weld	Tens	0.01	111	1	110	550	733.3	1.43	5000
S96_65_PBWJ_6	Plasma butt weld	Tens	0.01	101	1	100	500	666.7	1.48	5106
S96_65_PBWJ_7	Plasma butt weld	Tens	0.01	68.5	1	67.5	337.5	450	1.71	21,873
S96_65_PBWJ_8	Plasma butt weld	Tens	0.02	56.5	1	55.5	277.5	370	1.76	41,550
S96_SLJ_1	Lap joint ( $\alpha=0$ )	Tens	0.02	61	1	60	300	400	3.17	2057
S96_SLJ_2	Lap joint ( $\alpha=0$ )	Tens	0.05	21	1	20	100	133.3	3.37	81,463
S96_SLJ_3	Lap joint ( $\alpha=0$ )	Tens	0.02	41	1	40	200	266.7	3.35	8311
S96_SLJ_4	Lap joint ( $\alpha=0$ )	Tens	0.02	41	1	40	200	266.7	3.29	9333
S96_SLJ_5	Lap joint ( $\alpha=0$ )	Tens	0.05	21	1	20	100	133.3	3.33	96,320
S96_SLJ_6	Lap joint ( $\alpha=0$ )	Tens	0.03	31	1	30	150	200	3.16	26,096
S96_SLJ_7	Lap joint ( $\alpha=0$ )	Tens	0.02	61	1	60	300	400	3.29	1717
S96_SLJ_11	Lap joint ( $\alpha=0$ )	Comp	-41	-1	-41	40	266.7	200	4.21	102,684
S96_SLJ_12	Lap joint ( $\alpha=0$ )	Comp	-41	-1	-41	40	266.7	200	4.35	97,719
S96_SLJ_13	Lap joint ( $\alpha=0$ )	Comp	-48	-1	-48	47	313.3	235	n/a	917 <sup>b,c</sup>
S96_SLJ_14	Lap joint ( $\alpha=0$ )	Comp	-36	-1	-36	35	233.3	175	4.05	356,517
S96_SLJ_15	Lap joint ( $\alpha=0$ )	Comp	-36	-1	-36	35	233.3	175	3.96	326,296
S96_SLJ_16	Lap joint ( $\alpha=0$ )	Comp	-44	-1	-44	43	286.7	215	4.62	43,581
S96_SLJ_17	Lap joint ( $\alpha=0$ )	Comp	-44	-1	-44	43	286.7	215	n/a	17,489 <sup>c</sup>
S96_SLJ_21	Lap joint ( $\alpha=30^\circ$ )	Comp	0.02	-1	-44	43	286.7	215		64,990
S96_SLJ_22	Lap joint ( $\alpha=30^\circ$ )	Comp	0.02	-1	-44	43	286.7	215		60,864
S96_SLJ_23	Lap joint ( $\alpha=30^\circ$ )	Comp	0.02	-1	-41	40	266.7	200		109,716
S96_SLJ_24	Lap joint ( $\alpha=30^\circ$ )	Comp	0.02	-1	-41	40	266.7	200		124,620
S96_SLJ_25	Lap joint ( $\alpha=30^\circ$ )	Comp	0.03	-1	-36	35	233.3	175		293,841
S96_SLJ_26	Lap joint ( $\alpha=30^\circ$ )	Comp	0.03	-1	-36	35	233.3	175		206,033
S96_SLJ_32	Lap joint ( $\alpha=30^\circ$ )	Tens	-21	21	1	20	133.3	100		196,617
S96_SLJ_33	Lap joint ( $\alpha=30^\circ$ )	Tens	-41	41	1	40	266.7	200		13,917
S96_SLJ_34	Lap joint ( $\alpha=30^\circ$ )	Tens	-41	41	1	40	266.7	200		10,941
S96_SLJ_35	Lap joint ( $\alpha=30^\circ$ )	Tens	-31	31	1	30	200	150		36,318
S96_SLJ_36	Lap joint ( $\alpha=30^\circ$ )	Tens	-31	31	1	30	200	150		35,320

<sup>a</sup> $k_m = \Delta\sigma_s/\Delta\sigma_m$ , referring to the failure location. For the plasma butt welds and lap joints under compression,  $k_m$  refers to  $\Delta\sigma_{m,2}$  ( $t=3$ -mm plate). For the lap joints under tension,  $k_m$  refers to  $\Delta\sigma_{m,1}$  ( $t=4$ -mm plate)

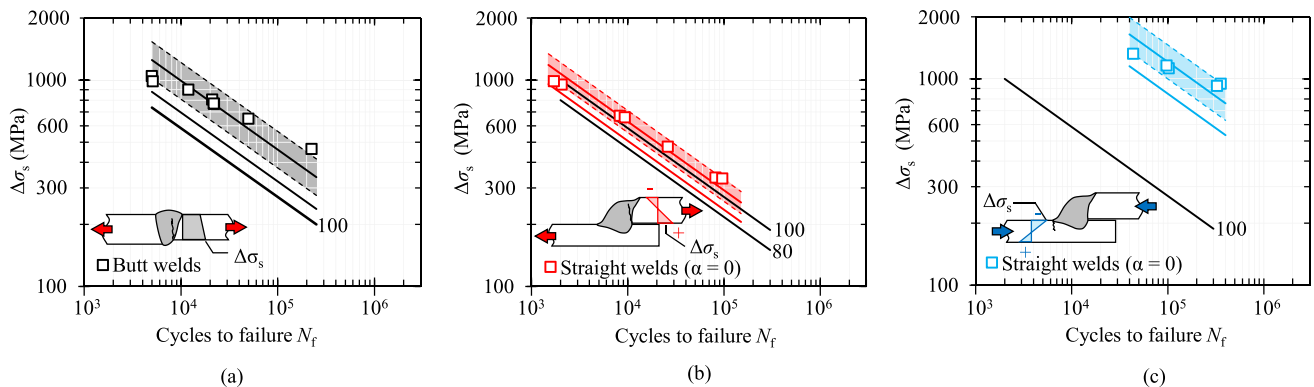
<sup>b</sup>Test interrupted, compressive maximum load close to the flexural buckling capacity of the specimen

<sup>c</sup>Fatigue strength limited by the flexural capacity of the specimen, not considered in the statistical analyses (see Section 3.2.3)

## Appendix 2. Fatigue test data presented with the fixed slope parameter ( $m = 3$ )



**Fig. 13** Fatigue test data and  $S$ - $N$  curves applying the fixed slope parameter of  $m = 3$  in the nominal stress system: **a** the plasma butt welds under tension, **b** lap joints under tension, and **c** lap joints under compression (details provided in Table 5, 6, and 7)



**Fig. 14** Fatigue test data and  $S$ - $N$  curves applying the fixed slope parameter of  $m = 3$  in the structural stress system: **a** the plasma butt welds under tension, **b** lap joints with the straight welds under tension, and **c** lap joints with the straight welds under compression (details provided in Table 5, 6, and 7)

### Author contribution

A. Ahola—conceptualization, formal analysis, investigation, methodology, validation, visualization, writing—original draft.  
 S. Salerto—investigation, validation.  
 T. Loisa—conceptualization, supervision, resources.  
 K. Lipiäinen—formal analysis, investigation.  
 T. Björk—conceptualization, supervision, resources, funding acquisition.

**Funding** Open Access funding provided by LUT University (previously Lappeenranta University of Technology (LUT)). The experimental work of this study has been carried out within the Intelligent Steel Applications (ISA) project (Grant ID, 7386/31/2018) with the support from Bronto Skylift Oy Ab. The reporting work has been finalized in the Fossil-Free Steel Applications (FOSSA) project (Grant ID, 5498/31/2021). The authors wish to thank the financial support of Business Finland in both projects.

**Data availability** Appendix 1 provides the details of fatigue test data applied in this work. Further necessary information can be made available upon request by contacting the corresponding author.

### Declarations

**Conflict of interest** The authors declare no competing interests.

**Open Access** This article is licensed under a Creative Commons Attribution 4.0 International License, which permits use, sharing, adaptation, distribution and reproduction in any medium or format, as long as you give appropriate credit to the original author(s) and the source, provide a link to the Creative Commons licence, and indicate if changes were made. The images or other third party material in this article are included in the article's Creative Commons licence, unless indicated otherwise in a credit line to the material. If material is not included in

the article's Creative Commons licence and your intended use is not permitted by statutory regulation or exceeds the permitted use, you will need to obtain permission directly from the copyright holder. To view a copy of this licence, visit <http://creativecommons.org/licenses/by/4.0/>.

## References

- Ban H, Shi G (2018) A review of research on high-strength steel structures. *Struct Build* 171:1600197. <https://doi.org/10.1680/jstbu.16.00197>
- Hwang I, Kim DY, Jeong G et al (2017) Effect of weld bead shape on the fatigue behavior of GMAW lap fillet joint in GA 590 MPa steel sheets. *Metals (Basel)* 7:1–12. <https://doi.org/10.3390/met7100399>
- Beretta S, Sala G (2005) A model for fatigue strength of welded lap joints. *Fatigue Fract Eng Mater Struct* 28:257–264. <https://doi.org/10.1111/j.1460-2695.2004.00849.x>
- Ahiale GK, Oh YJ, Choi WD et al (2013) Microstructure and fatigue resistance of high strength dual phase steel welded with gas metal arc welding and plasma arc welding processes. *Met Mater Int* 19:933–939. <https://doi.org/10.1007/s12540-013-5005-3>
- Yoshitake A, Kinoshita M, Osawa K et al (1994) Fatigue properties of fillet welded lap joints of high strength steel sheets for automobiles. *SAE Trans* 103:142–147. <https://doi.org/10.4271/940249>
- Shiozaki T, Yamaguchi N, Tamai Y et al (2018) Effect of weld toe geometry on fatigue life of lap fillet welded ultra-high strength steel joints. *Int J Fatigue* 116:409–420. <https://doi.org/10.1016/j.ijfatigue.2018.06.050>
- Matsuda K, Ishida Y, Kodama S (2023) Fatigue strength improvement method for thin sheet GMA welding joints by weaving. *Welding in the World* 67:733–739. <https://doi.org/10.1007/s40194-023-01480-z>
- Kim J, Lee K, Lee B (2011) Estimation of the fatigue life according to lap joint weld profiles for ferritic stainless steel. *Procedia engineering*. Elsevier Ltd, pp 1979–1984
- Wang Z, Wang Y, Gu H, Liao X (2023) Study on fatigue behavior and crack propagation life of longitudinal fillet welded lap joint. *Int J Fatigue* 167:. <https://doi.org/10.1016/j.ijfatigue.2022.107301>
- SSAB (2017) Technical data sheet of Strenx® 650MC D/E. 08/2017
- SSAB (2017) Technical data sheet of Strenx® 960MC. 04/2017
- voestalpine (2023) Technical data sheet of alform® x-treme, high-strength and ultra-high-strength heavy plates. 04/2023
- ESAB (2023) Technical data sheet of AristoRod 69. 12/2023
- Lincoln Electric (2023) Technical data sheet of ER70S-6 carbon steel welding wire
- Amraei M, Ahola A, Afkhami S, et al (2019) Effects of heat input on the mechanical properties of butt-welded high and ultra-high strength steels. *Eng Struct* 198:. <https://doi.org/10.1016/j.engstruct.2019.109460>
- EN 1011–1 (2009) Welding - recommendations for welding of metallic materials - Part 1: general guidance for arc welding. European Committee for Standardization, Brussels
- EN 1011–2 (2001) Welding - recommendations for welding of metallic materials. Part 2: arc welding of ferritic steels. European Committee for Standardization, Brussels
- Hobbacher A (2016) Recommendations for fatigue design of welded joints and components, 2nd edn. Springer International Publishing Switzerland, Cham
- Fricke W (2013) IIW guideline for the assessment of weld root fatigue. *Welding in the World* 57:753–791. <https://doi.org/10.1007/s40194-013-0066-y>

**Publisher's Note** Springer Nature remains neutral with regard to jurisdictional claims in published maps and institutional affiliations.